



Field Testing of Wind Turbine Towers with Contact and Noncontact Vibration Measurement Methods

Ying Wang¹; Kaoshan Dai, A.M.ASCE²; Yongfeng Xu³; Weidong Zhu⁴; Wensheng Lu⁵; Yuanfeng Shi⁶; Zhu Mei⁷; Songtao Xue⁸; and Karen Faulkner⁹

Abstract: Wind turbine tower vibration parameters are critical for design and maintenance of wind farms. In this paper, measurement campaigns of two in-service 65-m tall wind turbine towers are investigated. Different field vibration measurements with contact and noncontact sensors, including integrated circuits piezoelectric accelerometers, passive servovelocimeters, a laser Doppler vibrometer, and an interferometric radar, were conducted in the campaigns. Frequencies, damping ratios, and mode shapes were identified based on the measurements by use of a stochastic subspace identification method. Performances of the contact and noncontact sensors were compared in time and frequency domains. Also, time-frequency spectra were used to figure out noncontact measurement sections with high quality. Because the superior frequency ranges of contact and noncontact sensors are different, a data fusion method, which can take advantage of both types of sensors, was introduced. The practicality of field vibration measurements for modal parameter identification is discussed, and the results are compared with those from simplified finite-element models of the tested wind turbine towers. DOI: 10.1061/(ASCE)CF.1943-5509.0001366. © 2019 American Society of Civil Engineers.

Author keywords: Wind turbine tower; Field test; Modal analysis; Laser Doppler vibrometer; Interferometric radar.

Introduction

The wind power industry has developed rapidly in past decades, as wind turbines get taller and taller to maximize wind energy production. Wind turbine towers with increasing size and flexibility are subject to larger vibrations. Different structural problems related

to vibrations (e.g., material fatigue) have been gradually exposed along with the development of the industry (Chou and Tu 2011). To date, research performed on wind turbine towers mainly focuses on structural design (e.g., Dai et al. 2015, 2017a; Zhao et al. 2019), vibration control (e.g., Li et al. 2012; Zhang et al. 2019), and structural health monitoring (e.g., Hu et al. 2015a, b; Dai et al. 2017b). One critical objective of these research works is to establish a reliable understanding of the dynamic behavior of wind turbines.

The long-term monitoring of wind turbine towers has been performed with sensors that require physical components attached to the structure (Pieraccini et al. 2008; Swartz et al. 2010; Ozbek and Rixen 2013; Hu et al. 2015a, b). However, the deployment of contact vibration sensors is labor intensive and challenging from a logistical point of view. The height of most wind turbine towers combined with the lack of elevators hinders the deployment of sensors, data loggers, and computers needed in contact measurement methods. These also need long cables that increase the workload and the installation time unless wireless sensors are employed (Swartz et al. 2010). In addition, researchers that are not staff members of the wind farm often need permission and specific safety training to access a wind turbine tower and install the sensors.

Noncontact measurement methods can simplify significantly the field testing process, because there is no need to access the wind turbine (Pieraccini et al. 2008; Ozbek and Rixen 2013), although some measurement techniques may benefit from a reflection device attached to the structure to improve the quality of the signal (Ozbek and Rixen 2013). Noncontact measurement methods, such as photogrammetry systems, laser Doppler vibrometer (LDV), and interferometric radar (IR), have also been used in the testing of civil engineering structures (Brownjohn et al. 2017; Ozbek and Rixen 2013; Pieraccini 2013; Luzi et al. 2014; Gentile and Cabboi 2015).

Probably the most cost-effective method is the assembly of a photogrammetry system constructed with a consumer-grade camera and image processing, but it may be influenced by natural background lighting conditions (Brownjohn et al. 2017). Based on

¹Ph.D. Student, Dept. of Disaster Mitigation for Structures, Tongji Univ., Shanghai 200092, China. Email: tj_wangying@foxmail.com

²Professor, Ministry of Education Key Laboratory of Deep Underground Science and Engineering, College of Architecture and Environment, Sichuan Univ., Chengdu 610065, China; Professor, Dept. of Civil Engineering and Institute for Disaster Management and Reconstruction, Sichuan Univ., Chengdu 610065, China (corresponding author). ORCID: <https://orcid.org/0000-0002-0193-6076>. Email: kdai@scu.edu.cn

³Assistant Professor, Dept. of Mechanical and Materials Engineering, College of Applied Science and Engineering, Univ. of Cincinnati, Cincinnati, OH 45221. Email: xu2yf@ucmail.uc.edu

⁴Professor, Dept. of Mechanical Engineering, Univ. of Maryland, Baltimore, Baltimore, MD 21042. Email: wzhu@umbc.edu

⁵Professor, Dept. of Disaster Mitigation for Structures, Tongji Univ., Shanghai 200092, China. Email: wally@tongji.edu.cn

⁶Associate Professor, Ministry of Education Key Laboratory of Deep Underground Science and Engineering, College of Architecture and Environment, Sichuan Univ., Chengdu 610065, China. Email: shiyuanfeng@scu.edu.cn

⁷Assistant Professor, Ministry of Education Key Laboratory of Deep Underground Science and Engineering, College of Architecture and Environment, Sichuan Univ., Chengdu 610065, China. Email: zhu.mei@scu.edu.cn

⁸Professor, Dept. of Disaster Mitigation for Structures, Tongji Univ., Shanghai 200092, China. Email: xue@tongji.edu.cn

⁹Ph.D. Student, College of Engineering, Mathematics and Physical Sciences, Univ. of Exeter, Exeter, Devon EX4 4QF, UK. Email: kf312@exeter.ac.uk

Note. This manuscript was submitted on January 2, 2019; approved on May 20, 2019; published online on November 12, 2019. Discussion period open until April 12, 2020; separate discussions must be submitted for individual papers. This paper is part of the *Journal of Performance of Constructed Facilities*, © ASCE, ISSN 0887-3828.

Doppler shifts of a laser beam, laser vibrometers have been used in operational modal analysis of wind turbine towers (Ozbek and Rixen 2013; Dai et al. 2015). However, current LDV sensors can only measure from a single point. IR sensors, which are not influenced by weather conditions, have been used in field testing of historic buildings, television towers, and stay cables (Pieraccini 2013; Luzzi et al. 2014; Gentile and Cabboi 2015). Although many vibration sensors have been used in field tests of wind turbine towers, their performance in this area have not been compared and discussed.

The objective of this paper is to investigate different contact and noncontact vibration measurement methods for wind turbine towers. These methods include integrated circuits piezoelectric (IEPE) accelerometers, passive servo (PS) ultra-low frequency velocimeters, LDV sensors, and IR sensors. Experimental studies were conducted on two in-service wind turbine towers, which were located at two different wind farms in Shanghai (Tower A) and Jiangsu (Tower B), China, respectively. Vibration measurements collected by different sensors were analyzed and compared in both time and frequency domains. Modal parameters of both towers were identified by using a stochastic subspace identification (SSI) method. The results were also compared with those obtained from simplified finite-element (FE) models of wind turbine towers.

Vibration Sensing

Contact Sensors

IEPE accelerometers and PS velocimeters were used for wind turbine tower measurements. The IEPE accelerometers was a LC0132T model sensor (Lance Measurement Technologies, Hebei, China) It is a type of sensor that use piezoelectric crystals as transducers and integrated circuits to reduce measurement noise by shortening distances from amplifiers. The transducer of a PS velocimeter is a 941B model sensor (Institute of Engineering Mechanics, China Earthquake Administration, Beijing). It is a moving coil that uses servotechnology to extend the equivalent mass of the pendulum, thus enlarging the measurement range in the lower-frequency range with the same level or error (Yang et al. 2005). Details of the sensors used are presented in Table 1. Only parameters of the medium velocity mode of the PS velocimeters used in this work are given in the table.

Noncontact Sensors

Two kinds of noncontact sensors were used in field tests. One was a RSV-150 remote sensing LDV sensor (Polytec, Waldbronn, Germany), and the other one was an IBIS-FS IR sensor (IDS GeoRadar, Pisa, Italy).

Table 1. Details of contact sensors used for two wind turbine tower measurements

Item	Tower A	Tower B
Type	Integrated circuits piezoelectric	Passive servo
Sensitivity	40 V/g	2.4 V/(m/s)
Resolution	5×10^{-7} g	4×10^{-7} m/s
Frequency range	0.5–1,000 Hz ($\pm 10\%$) ^a	0.25 ~ 100 Hz (+1 ~ -3 dB) ^a
Measurement range	0.12 g	0.3 m/s
Weight	310 g	750 g

^aFrequency range that can be measured at this error level.

The LDV sensor is a single point sensor in which a laser beam is focused onto a vibrating target and modulates the laser frequency through the Doppler effect. A fraction of the modulated beam is scattered back and collected by the long-range lens. Inside the sensor, an interferometer is used to extract the modulation and transfer it into velocity or displacement of the vibrating target (Polytec Inc. 2017). The LDV sensor used in this work translates the modulation into velocity, and its installation time is around 10 min. Some technical parameters of the LDV sensor are listed in Table 2.

The LDV sensor does not strictly require any device attached to the structure being tested; however, the quality of the measurements benefit from the installation of a reflecting device, such as a reflector or a total-reflecting prism. Operational conditions also affect the LDV sensor's performance, e.g., low temperature and direct sunlight. Another challenge is keeping the laser beam on the target and, although different scanning or sensor types can be used, focusing the laser point on the target surface at different distance ranges can still be problematic.

The IR sensor uses microwaves to measure the displacement of the target, which is obtained by extracting the phase difference between the incident and the reflected microwaves (Pieraccini 2013). Like the LDV sensor, reflection devices are not strictly necessary but can help improving measurement quality. Unlike the LDV sensor, the IR sensor can be used for multipoint measurements, and it does not need focusing. The sensor parameters of the IR sensor are presented in Table 2.

Contact sensors have been validated in many cases but, unless this technology is used for long-term or permanent monitoring, it is not generally suitable in rapid field testing of wind turbine towers, because the required equipment (including sensors, cables, data loggers, and computers) is difficult to deploy. On the other hand, noncontact sensors, like LDV and IR sensors, are easy to set up and, therefore, are more suitable for field tests. From a cost perspective, LDV or IR sensors are one or two orders of magnitude more expensive than contact sensors (including the data logging system).

Field Tests

Wind Turbine Towers

Vibrations of two in-service wind turbine towers under ambient excitation were measured. Tower A carried an S70 1.5 MW three-blade horizontal axis wind turbine (Nordex, Hamburg, Germany) and was located in Shanghai, China. The tower was tapered and tubular with bottom and top diameters of 4.04 and 2.96 m, respectively. The height between the turbine hub and the ground was 65 m. For Tower A, the IEPE accelerometers, LDV, and IR sensors were used to measure its vibration. Note that the measurements were taken on different days with no overlaps.

Tower B carried an SL1577 wind turbine (Sinovel, Beijing) which was also a 1.5 MW three-bladed horizontal axis turbine

Table 2. Parameters of LDV (RSV-150) and IR (IBIS-FS) sensors

Item	LDV sensor	IR sensor
Long range	5 ~ 300 m depending on target reflectivity and amplitude	0.01 ~ 2.0 km depending on target reflectivity and amplitude
Resolution	$< 0.5 \mu\text{m/s/Hz}^{1/2}$	0.01 mm
Frequency range	0 ~ 25 kHz	0 ~ 200 Hz
Weight	Approximate 30 kg, including storage case, excluding tripod	20 kg

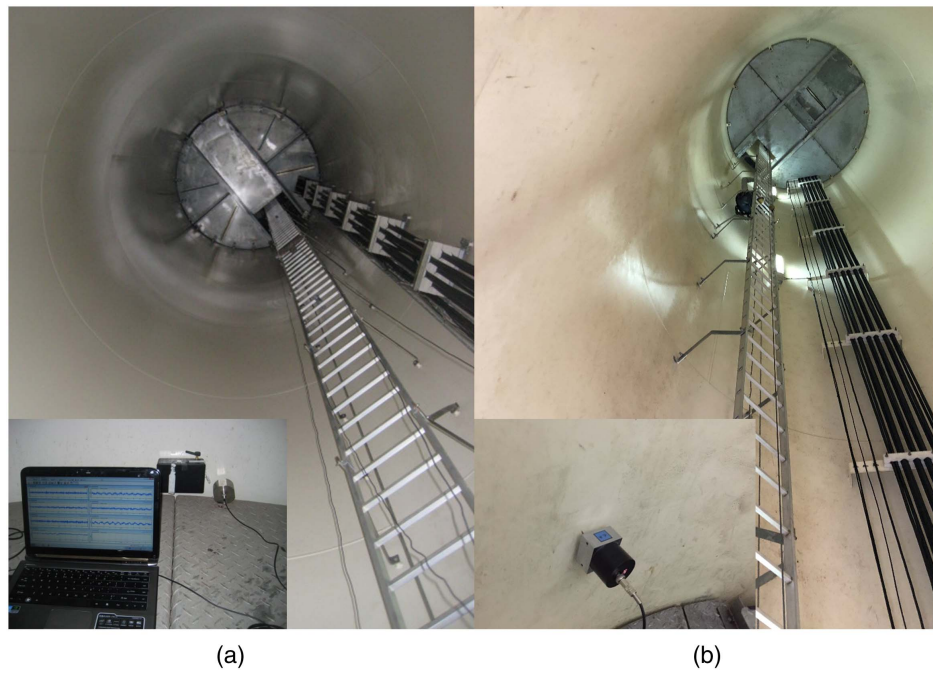


Fig. 1. Interior of wind turbine towers and deployment of the sensors: (a) Tower A; and (b) Tower B.

Table 3. Heights of platforms in which accelerometers were deployed

Platform	Tower A	Tower B
Platform 1	—	16.4 m
Platform 2	34.6 m	38.8 m
Platform 3	50.8 m	60.8 m
Platform 4	—	—
Platform 5	61.4 m	—

and was located in Jiangsu, China. The tower was tapered and tubular with bottom and top diameters of 4.00 and 2.40 m, respectively. The height between the turbine hub and the ground was 65 m. The equipment used in for testing included PS velocimeters as well as the same model LDV and IR sensors as for Tower A.

All vibration measurements were taken when the wind turbines were parked, and they were referred to as (or transferred into) the horizontal movement of the tower except for the LDV

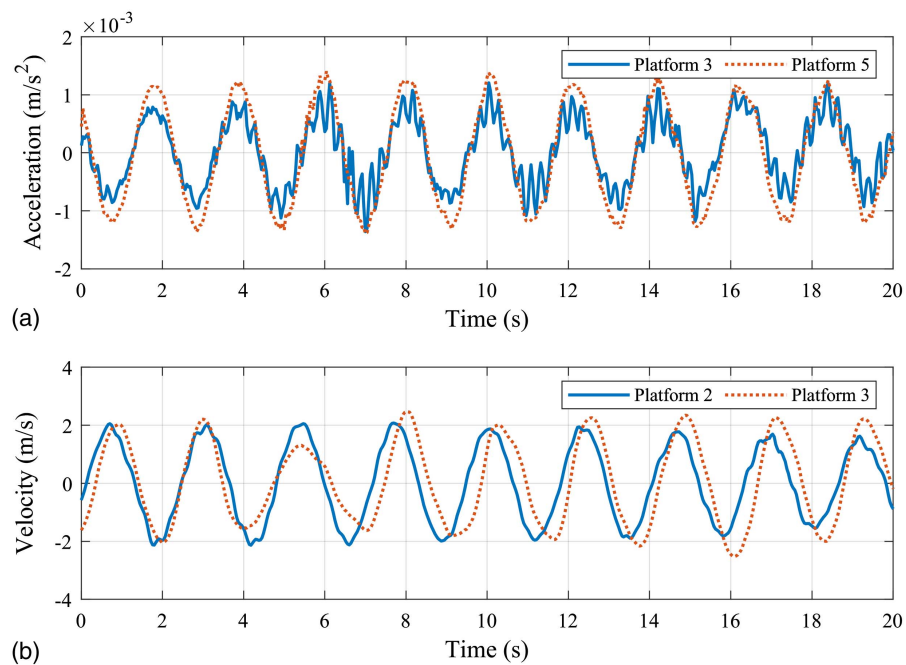


Fig. 2. Vibration measurements at different platforms obtained with contact sensors: (a) IEPE acceleration measurements in Tower A; and (b) PS velocity measurements in Tower B.

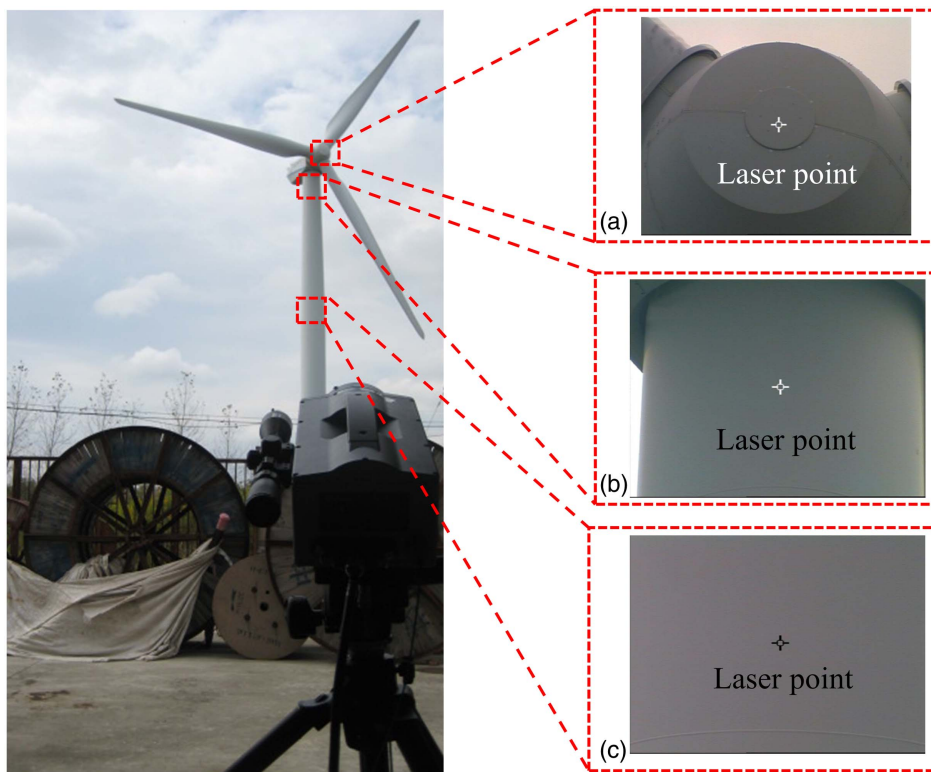


Fig. 3. LDV measurement positions on Tower A: (a) hub level; (b) top—tower; and (c) midtower.

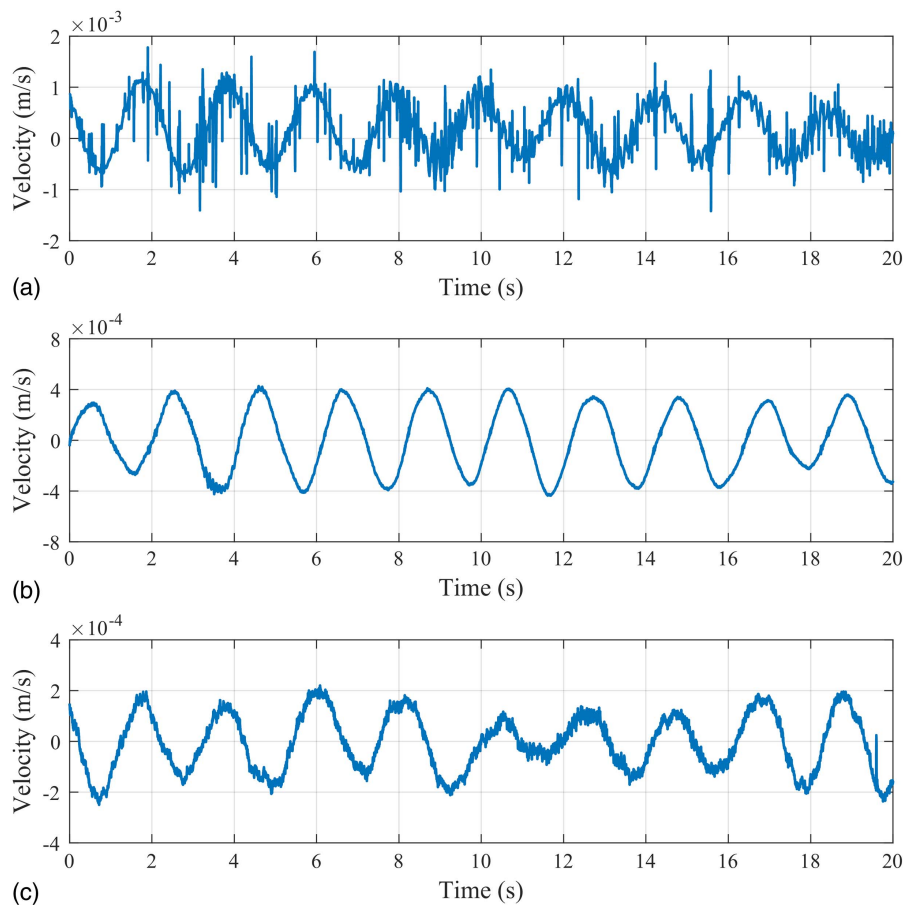


Fig. 4. Velocity time histories of Tower A measured with LDV sensor: (a) hub level; (b) top—tower; and (c) midtower.

measurements, which were in the direction along the laser beam. The IEPE accelerometers and the LDV sensor measured the vibration of Tower A in the horizontal direction parallel to the plane of the blade plane and perpendicular to it. However, the IR sensor measured the horizontal movement in no specific direction due to limitations in the space required to set up its equipment. For Tower B, the direction of PS velocimeters were set to match the IR measurement direction.

Measurements with Contact Vibration Sensors

The vibrations of Tower A were measured with IEPE accelerometers in 10-min durations and a sampling frequency of 100 Hz. For Tower B measurements, PS velocimeters were used with a sampling frequency of 25.6 Hz and a duration of 20 min. Fig. 1 shows the interior of both wind turbine towers and how the sensors were attached to the tower wall by means of magnetic bases. The

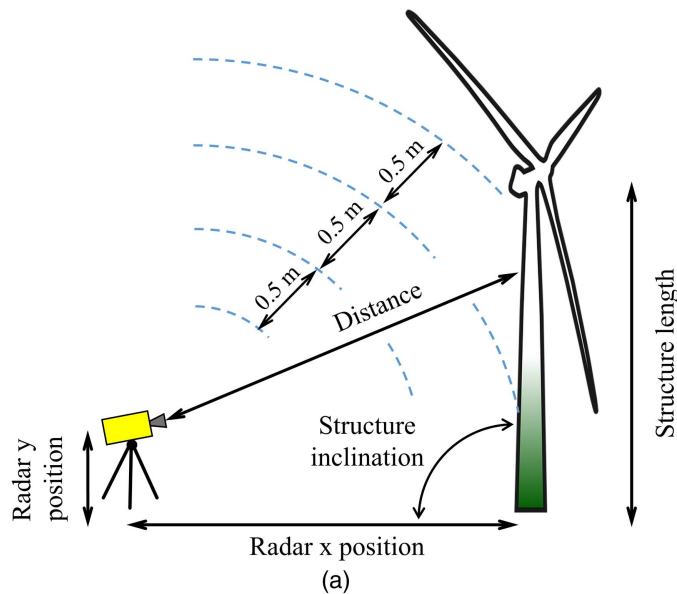


Fig. 5. Field testing with use of IR sensor: (a) IR measurement and test setups; (b) Tower A; and (c) Tower B.

sensors were located at maintenance platforms in wind turbine towers, and their heights are shown in Table 3. Although the sensors were deployed in three platforms of each tower, no more than two platforms were used together at the same time due to the limitations of cables and number of sensors. Fig. 2 shows typical time histories of the vibration measurements in the two towers.

Measurements with LDV Sensor

Vibrations at three points of Tower A were measured by the LDV sensor: a hub level point, a top-tower point, and a mid-tower point, as shown in Fig. 3. The exact heights of the measured point locations are unknown because the distance between the LDV sensor and the tower could not be accurately measured because of blocks, such as plants and bobbins on the ground, as shown in Fig. 3. One of the advantages of the LDV sensor is its high sampling frequency. However, the dominant vibration frequencies of a wind turbine tower are usually under 5 Hz (and correspond to the first two vibration modes). Thus, the sampling frequency was set as the lower limit of the LDV sensor, which is 240 Hz. The duration of the measurements was around 10 mins. Typical time histories of the vibration measured with the LDV sensor at the three points are shown in Fig. 4, the measurement at the hub-level point height is fuzzy possibly due to the poor reflection condition of the hub and the sufficiently small angle between the laser beam and the reflection surface. The same type of LDV sensor was used in Tower B, but the strength of the reflection signal was not enough to obtain valid data. The reason could be that the temperature was occasionally below 5°C during testing of Tower B, and this is out of the operational temperature range of the LDV sensor: 5°C–40°C.

Measurements with IR Sensor

Fig. 5 shows test setups for the two towers with IR sensors. Vibrations of the two towers were measured by the IR sensor. Due to the characteristics of the IR sensor, measurements at locations spaced

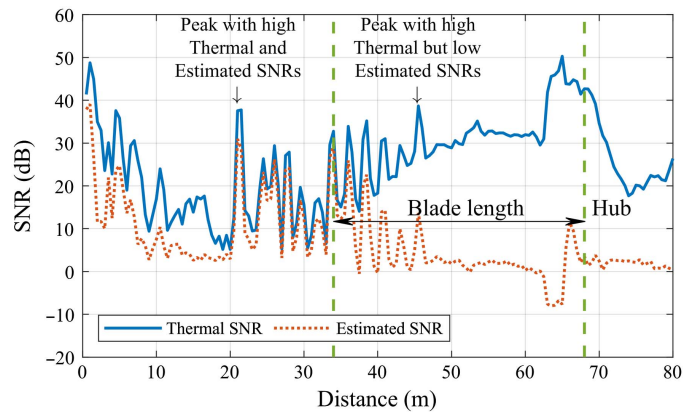


Fig. 6. Typical thermal and estimated S/N ratios in IR measurements of Tower B.

Table 4. Geometry settings of IR measurements

Item	Tower A	Tower B
Structure length	65 m	60 m
Structure inclination	90°	90°
Radar x position	21 m	20.5 m
Radar y position	3 m	0 m

Note: Length and IR positions are shown in Fig. 5(a).

every 0.5 m along the distance from the sensor to the tower were recorded; however, a number of these were not usable, because they were not reflected by the structure, or they were of low quality. The quality of IR measurements can be assessed by two indices (IDS

GeoRadar Inc. 2016): (1) the thermal signal-to-noise (S/N) ratio, which is a value that is related to the power received from each measurement point; and (2) the estimated S/N ratio (SNR), which is a value that is related to the real noise that affects the

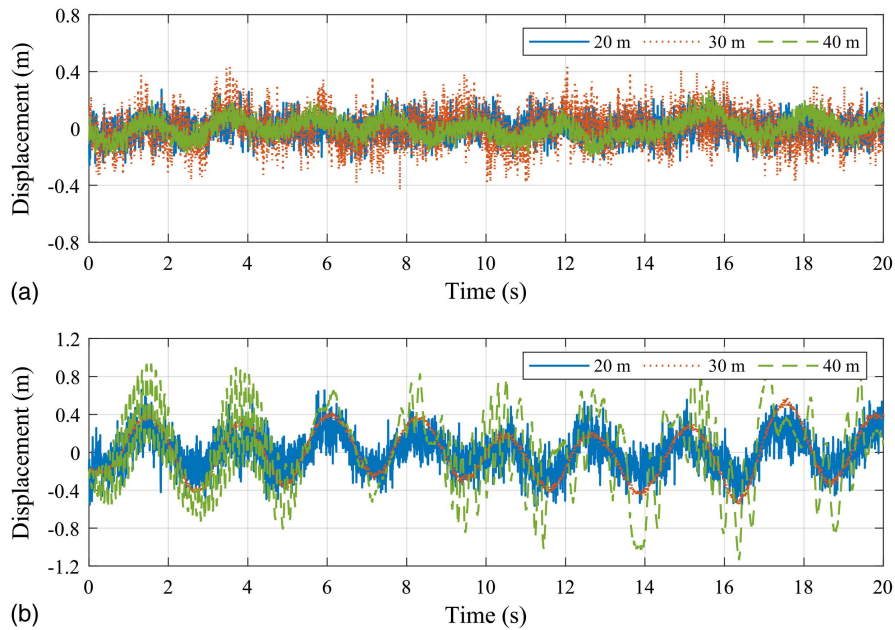


Fig. 7. Displacement time histories measured with IR sensor at different heights of wind turbine tower: (a) Tower A; and (b) Tower B.

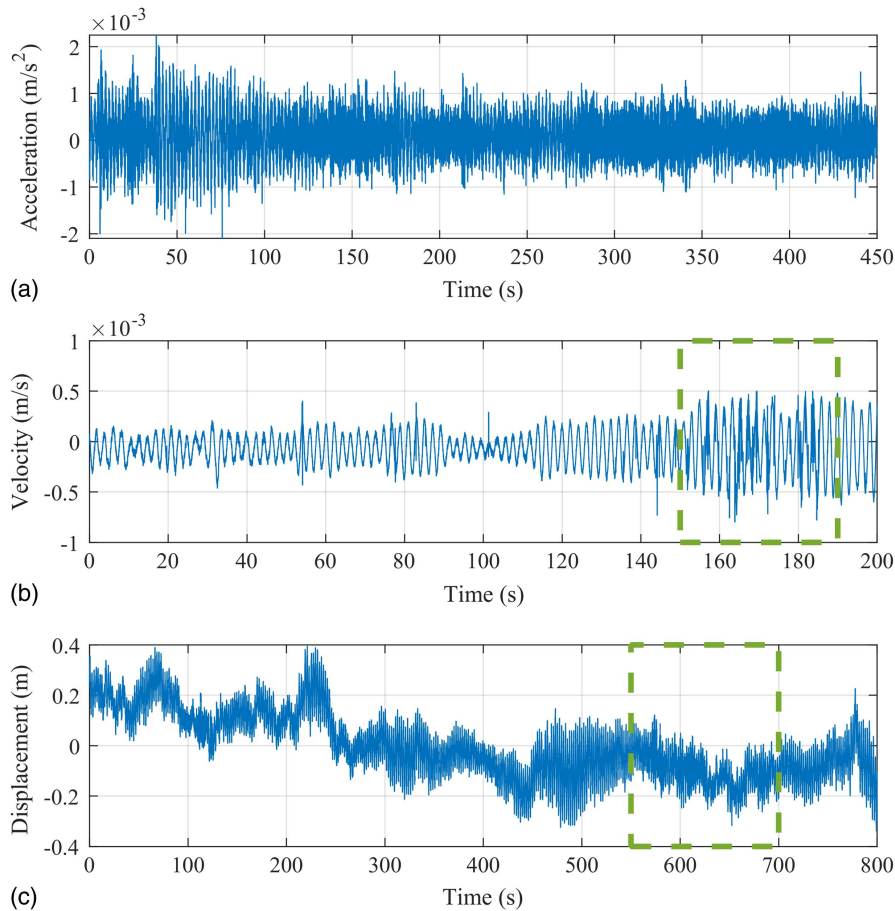


Fig. 8. Vibration time histories recorded in middle level of Tower A: (a) IEPE accelerometers (Platform 2); (b) LDV sensor (midtower point); and (c) IR sensor (34.6 m).

measurement of each measurement point during the survey. These two S/N ratios are calculated by the corresponding software. The recorded data is considered valid when the peaks in thermal and estimated S/N ratios occur at the same distances, and their S/N ratios are relatively high. The data from the middle and the lower parts (under 40-m height) of the two towers were more reliable, according to the S/N ratios. The reason is that the signal corresponding to the tower top can be influenced by the blades and the elevation angle of the IR sensor. Fig. 6 shows typical thermal and estimated S/N ratios. The height of the location corresponding to each measurement can also be calculated with the distance between the measurement point and the sensor, and with the distance between the tower and the sensor, according to trigonometric functions (the geometric settings of the sensor are given in Table 4, and measurements will be transferred into the horizontal direction by the logging software with these settings). The sampling frequency was set as 200 Hz (upper limit of the IR sensor) and the duration of each measurement was 15 min. Typical time histories of measurements obtained with the IR sensor are shown in Fig. 7.

IR sensors can simultaneously measure displacements of several points, which allows one to efficiently capture vibration mode shapes of a structure. However, the vibration at the top of the towers (above 40 m) could not be obtained with the IR sensor for either Tower A or B. Furthermore, the amplitudes of higher order modes can be lower than the sensing range of the IR sensor and thus may be submerged in background noises. The IR sensor can give a dense map of points with valid measurements at certain parts of the wind turbine tower, but they may not be helpful to identify important vibration modes, because the data may be redundant. Consequently, valid measurements should be selected prior to further data processing, but doing so may complicate data processing.

Measurement Comparisons

Qualities of measurements obtained by the different kinds of sensors are compared in this section, and several mainstream data processing methods are used to check data quality. In sections “Signal Quality of Tower A Measurements” and “Signal Quality of

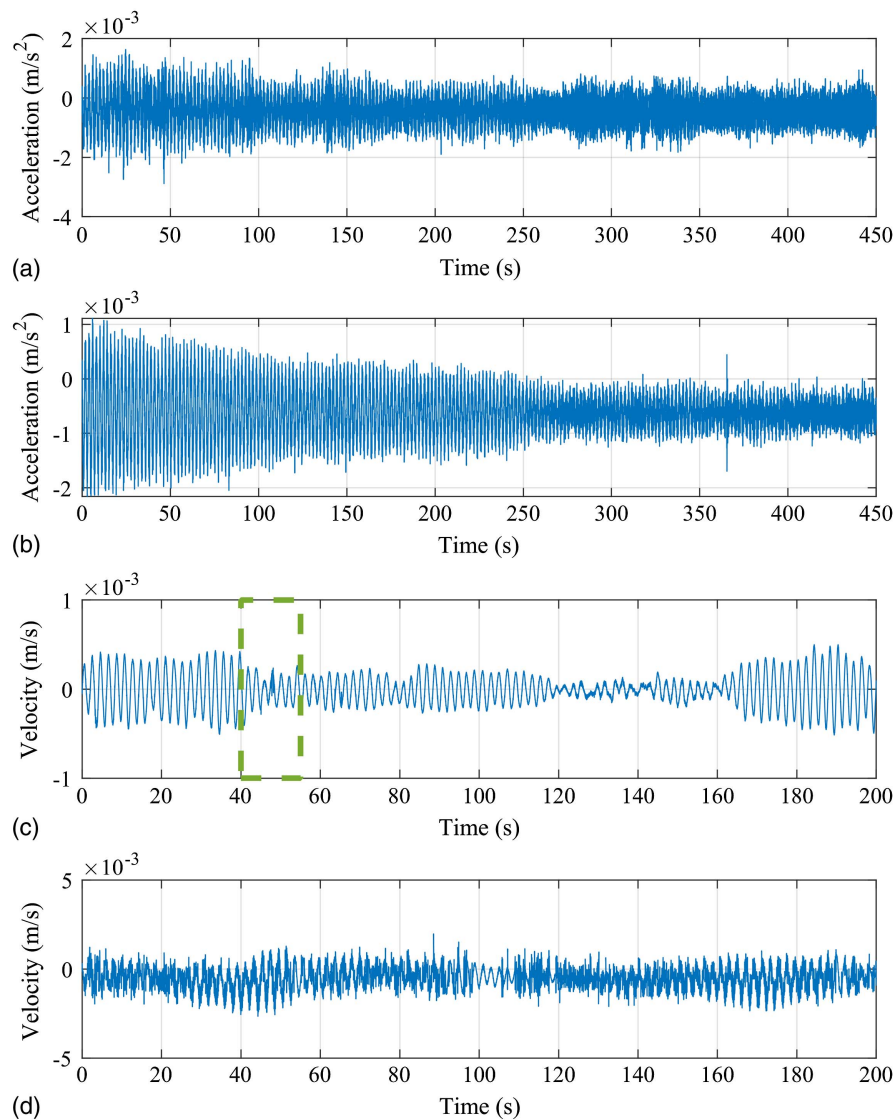


Fig. 9. Vibration time histories measured at top and hub level of Tower A: (a) IEPE accelerometers (Platform 3); (b) IEPE accelerometers (Platform 5); (c) LDV sensor (top-tower point); and (d) LDV sensor (hub-level point).

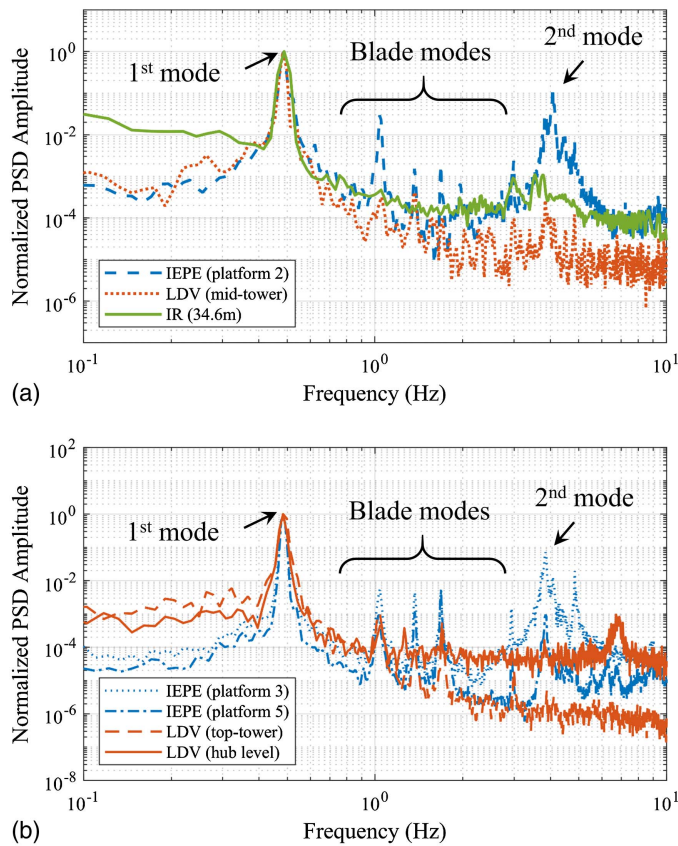


Fig. 10. Normalized PSDs of vibration of Tower A: (a) midtower height; and (b) top-tower height.

Tower B Measurements,” measurements of Towers A and B will be compared in time, frequency, and time-frequency domains. In section “Data Fusion of Displacement and Velocity Signal,” a data fusion (DF) method is introduced, because it takes advantage of both contact and noncontact sensors by combining their superior frequency ranges thus getting the full range of vibration for a structure. In section “Modal Analysis” that follows, modal identification, which is the most primary usage of structural vibration measurements, is also applied with the obtained measurements.

Signal Quality of Tower A Measurements

Figs. 8 and 9 show typical vibration time histories recorded in the middle and the top of Tower A, respectively. No valid data could be recorded with the IR sensor above a height of 40 m. For this reason, these results are omitted in Fig. 9. The measurements were taken on different days, and they were subject to wind with different speeds and directions. Hence, the measurements could not be compared directly with others in their original amplitudes. Thus, all the power spectral densities (PSD) were normalized by dividing them by the values corresponding to the first peaks so that the frequency positions of the peaks in the PSD plots could be compared. The same measurements are presented Figs. 10 and 11 in the frequency domain in and in their original scale and velocity scale, respectively. In Figs. 10 and 11, the PSDs of each measurement are normalized by dividing the amplitude associated with each corresponding to the first peak (at the frequency of 0.49 Hz). As shown in Fig. 10(a), the positions of the peaks in the PSDs corresponding to the IEPE accelerometers and the LDV sensor agree well with one another at the first and the blade modes frequencies. Note that the LDV sensor

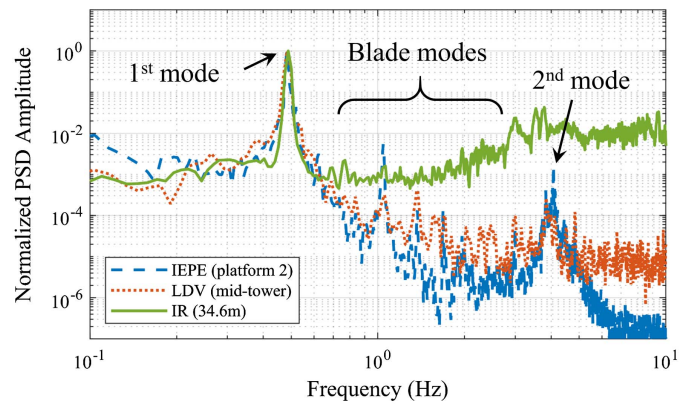


Fig. 11. Normalized PSDs of vibration recorded at middle of Tower A (in velocity scale).

measured velocities, and the IR sensor measured displacements. Hence, the PSD values in their original scales, shown in Fig. 10(a), had different amplifications. Fig. 10(b) compares the PSDs obtained from IEPE and LDV measurements (in their original scales, namely, acceleration and velocity, respectively) at the top of Tower A, and it shows, once again, that the first vibration frequency clearly coincided in both cases.

Fig. 11 compares the frequency content of the tower velocity signals processed from the measurements obtained with the IEPE accelerometers (time-integration signal), the LDV sensor (direct signal), and the IR sensor (time-derivation signal). The integration of IEPE measurements used here follows the trapezoidal rule, and the derivation was obtained as the slope of the consecutive displacement measurements. The first mode was well captured regardless of the type of signal considered in the PSD (acceleration, velocity, or displacement), but the contribution of higher-order modes obtained from the IEPE accelerometers and the LDV sensor was more consistent if the PSD was plotted in velocity scale. The frequency content above the first frequency obtained with the IR sensor differed from the rest of the sensors. This was attributed to the fact that the displacement measurement resolution of the IR IBIS-FS sensor is 0.01 mm. Consequently, the modes with vibration amplitudes less than this threshold, which was usually the case in high-order modes, could not be detected with the IR sensor.

Time-frequency spectra were also obtained from the recorded signals by means of the short-time Fourier transform (STFT), as shown in Figs. 12 and 13. The spectra obtained from IEPE and LDV measurements are clearer in the lines corresponding to the second vibration mode of the tower (close to 4 Hz). The dash-line boxes in Figs. 12 and 13 highlight time-intervals of abnormal energy content corresponding to broadband noise (vertical lines in time-frequency spectra), which are observed only with the noncontact measurement techniques (i.e., LDV and IR). The corresponding time-intervals are also remarked with the dash-line boxes in the time history diagrams included in Figs. 8 and 9, which show that certain noise was present at those intervals. This result suggests that poor signal returns obtained in noncontact sensing techniques can lead to deviations in the time-frequency spectra, but these are filtered out when the PSD of the whole signal is obtained, as shown in Figs. 10 and 11.

Signal Quality of Tower B Measurements

For Tower B, the data were obtained with over 10 min overlaps (measurements corresponding to the same period) for each sensor.

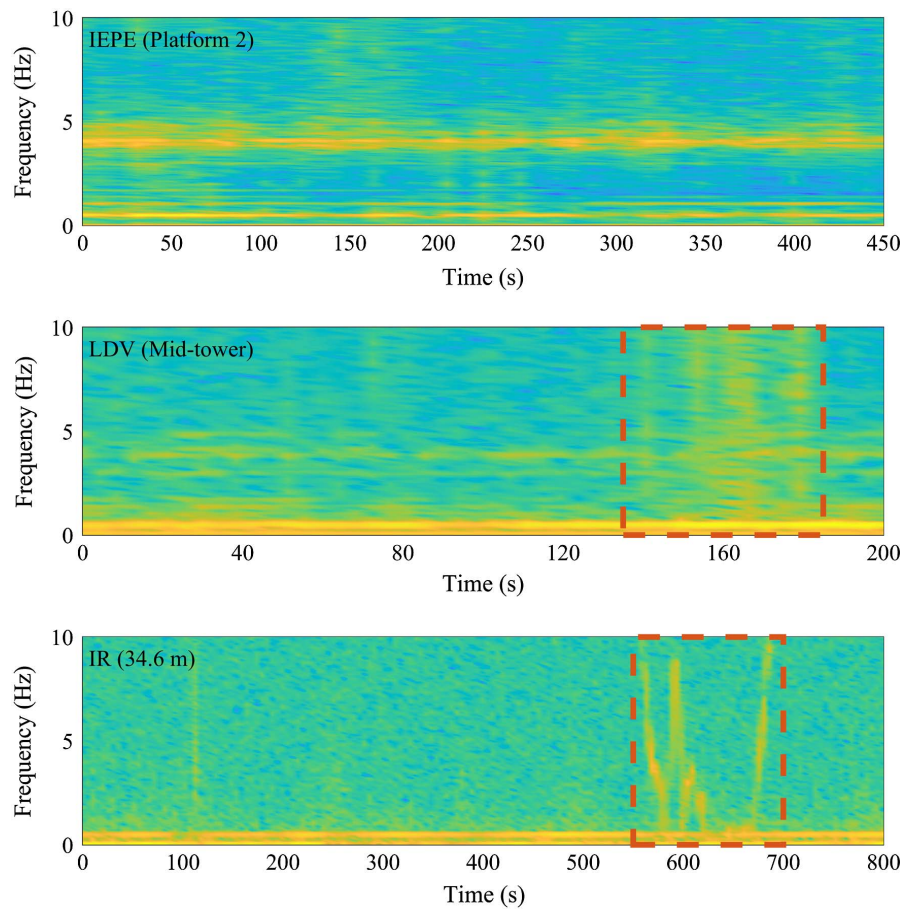


Fig. 12. Time-frequency domain comparison of measurements at middle height of Tower A. First, second, and third rows correspond to measurements obtained from IEPE accelerometers, LDV sensor, and IR sensor, respectively.

The measurement directions of the PS velocimeters and the IR sensor were set as the same. No valid LDV data could be obtained in the field tests of this tower. A maximum correlation method was used to estimate the delays between the signals. In this method, the normalized cross-correlation between the time-integrated PS measurement and the original IR measurement was calculated, and the estimated delay was given by the negative of the lag for which the normalized cross-correlation had the largest absolute value. The calculated time between PS and IR measurements agreed well with the recorded measuring times. For Platform 1, the starting time of the PS measurement was 6:37 p.m. and that of the IR measurement was 6:45 p.m. on the same day. For Platform 2, the starting time of the PS measurement was 3:46 p.m. and that of the IR measurement was 3:53 p.m. By using the maximum correlation method, the calculated time delays were 8.67 and 7.24 min for Platforms 1 and 2, respectively. The synchronized time histories of Tower B measurements are shown in Fig. 14, which includes the measurements from the IR sensor and the PS velocimeters.

The time histories were converted to the frequency domain and are shown in Fig. 15, where the PSD curves are plotted in their original units. The IR measurement had only one dominant peak that corresponded to the first vibration mode at 0.43 Hz. Contact vibration sensors (i.e., PS velocimeters) showed a better performance in the high frequency range of the tower vibration again. The time-frequency spectra of Tower B measurements presented in Fig. 16 show that the IR measurements at the height of 39.8 m contained several abnormal lines, indicating the presence of high-frequency noise in the recorded signal. However, this was not

observed in the records obtained by the IR sensor at a lower position on the tower (16.9 m height), because the signal had better quality. This agrees well with the S/N diagram in Fig. 6.

In summary, contact vibration sensors, including IEPE accelerometers, PS velocimeters, and LDV sensors were found to have better performance when measuring high-order frequencies than IR sensors. Although contact vibration sensors with good low-frequency performances were used, i.e., the PS velocimeter, the lower frequency content of the tower vibration could still be missing. Although both LDV and IR sensors are active vibration sensors, which use self-generated electromagnetic waves, the quality of the signals is significantly influenced by environmental factors. A time-frequency spectrum can assist with picking measurements sections with the best quality.

Fig. 17 compares a typical trapezoidal integration of the PS and original the IR measurements. The recorded displacements followed the same trends for both sensors, and they clearly showed that the distance between the consecutive peaks, which is related to the period of the first vibration mode, was the same. However, the magnitude of the tower displacements recorded by the IR sensor was significantly larger than those obtained from the accelerometer, in some cases more than double. This may be due to low frequency (below 0.25 Hz) components of the vibration induced by wind during testing, which could have affected the amplitude of the displacements measured by the IR sensor but not by the contact sensors, because the wind-induced motion was below 0.25 Hz (i.e., the lower-bound frequency of the PS velocimeter).

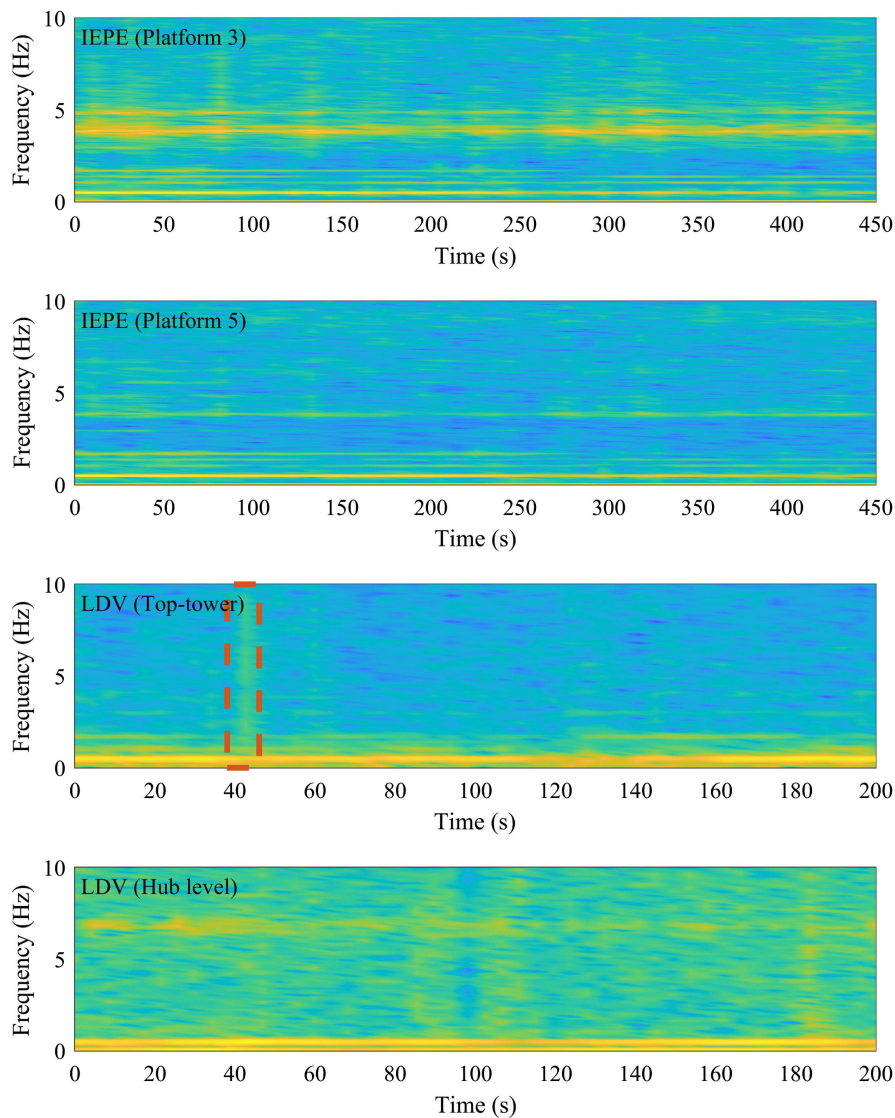


Fig. 13. Time-frequency domain comparisons of measurements at top of Tower A. First two rows correspond to measurements obtained from IEPPE accelerometers (at different heights); last two rows correspond to LDV measurements.

Data Fusion of Displacement and Velocity Signals

In sections “Signal Quality of Tower A Measurements” and “Signal Quality of Tower B Measurements,” contact sensors were shown to have a good performance in the high-frequency region, and the noncontact sensors were shown to have better accuracy in the low-frequency region. To take advantage of both contact and non-contact sensors, i.e., merge the low-frequency measurements of noncontact sensor with the high-frequency of contact sensor measurements, DF methods were used. This section proposes the use of the DF method based on the Kalman filter. This method was recently presented by Kim and Sohn (2017), and it was applied to wind turbine vibration measurements in this study to achieve a high-precision measurement of tower displacement. Let a state vector be defined as

$$\mathbf{x}(k) = \begin{Bmatrix} x(k) \\ \epsilon(k) \end{Bmatrix} \quad (1)$$

where $x(k)$ = displacement at the k th time point; and $\epsilon(k)$ is assumed to be a piecewise constant that is used to complete the state

space model. A state-space model that can be used for displacement and velocity DF can be expressed as

$$\mathbf{x}(k+1) = \mathbf{A}\mathbf{x}(k) + \mathbf{B}(\dot{x}_m(k) + w(k)) \quad (2)$$

$$x_m(k) = \mathbf{C}\mathbf{x}(k) + v(k) \quad (3)$$

where $\mathbf{A} = \begin{bmatrix} 1 & \Delta t \\ 0 & 1 \end{bmatrix}$, $\mathbf{B} = \begin{bmatrix} \Delta t \\ 0 \end{bmatrix}$, and $\mathbf{C} = [1 \ 0]$ = matrices that describe the state-space problem; and $w(k)$ and $v(k)$ = white-noise Gaussian processes, and their variances are set as 4×10^{-7} m/s and 1×10^{-5} m based on sensor resolutions (Tables 1 and 2).

Figs. 18 and 19 show the displacement measurements obtained from the IR sensor and from the PS velocimeter in the time and frequency domains. These figures also compare the original measurements with the fused high-frequency components of contact sensor measurements and the low-frequency components of non-contact sensor measurements. The DF estimation brought the integrated PS measurements significantly closer to those obtained with the IR sensor. Although some differences remained between both

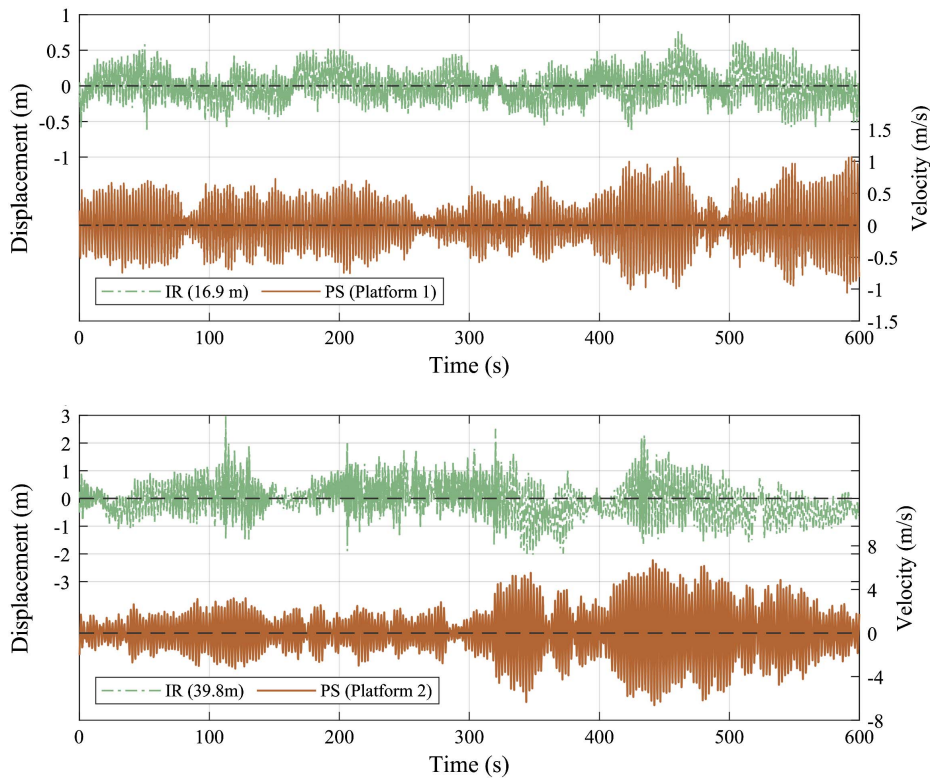


Fig. 14. Synchronized time histories of Tower B vibration at different heights.

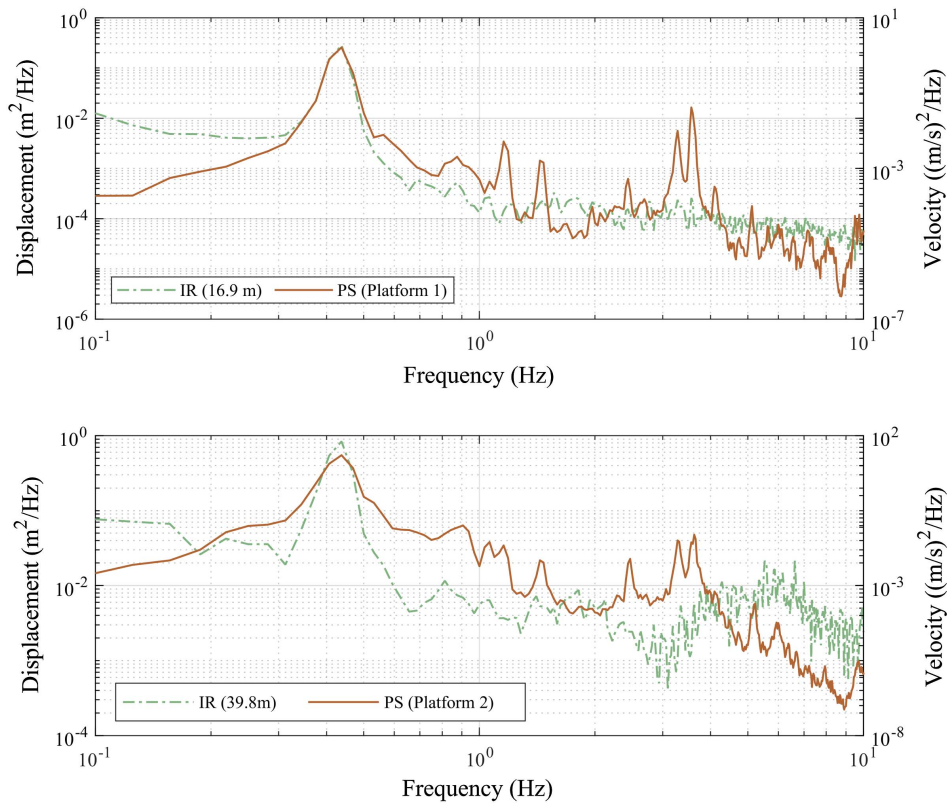


Fig. 15. Frequency content of Tower B vibration at different positions.

measurement methods in the time domain, the DF estimations captured reasonably well the high-frequency range of the tower vibration (above 0.43 Hz), because it was close to the frequency content obtained only with the accelerometer in this range. The

IR measurements were smoothed in the high-frequency range with the DF process whilst retaining the low frequency components of the IR measurement (below than 0.25 Hz). The results demonstrate that fusing measurements from contact and noncontact

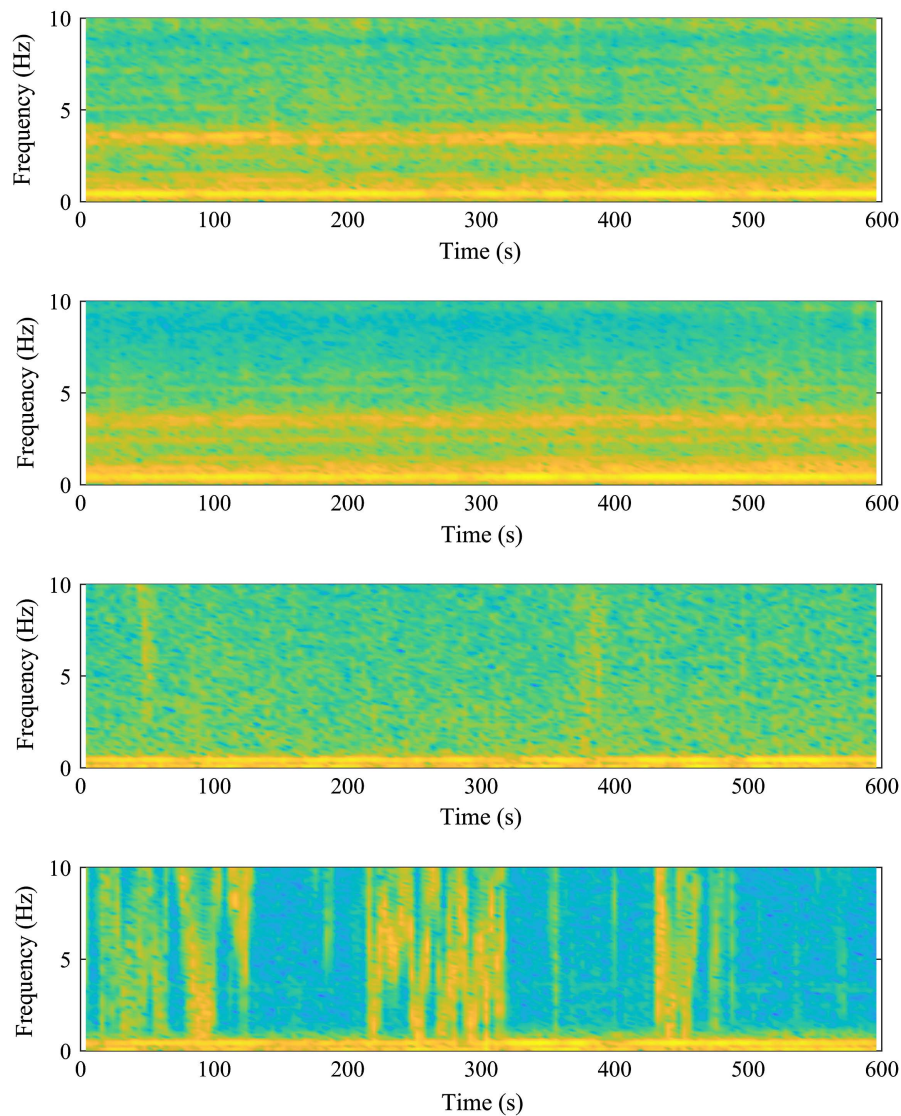


Fig. 16. STFT spectra of measurements in Tower B. First two rows correspond to measurements obtained from PS velocimeter (at different heights); last two rows correspond to IR sensor.

measurements can result in a fused signal that is accurate in a broad range of frequencies.

Modal Analysis

The modal parameters of both wind turbine towers were estimated with a data-driven SSI method (Van Overschee and De Moor 1993; Golub and Van Loan 1996; Peeters and De Roeck 1999). Stability diagrams of both towers from the SSI method are shown in Figs. 20–23. Each line in the stability diagrams corresponds to a vibration mode of the structure. A total of 30 calculation orders was considered. The modal identification was performed based on the measurements obtained with the IEPE accelerometers, the PS velocimeters, the LDV sensor, and the IR sensor. Although several sections were measured with the contact vibration sensors, the acceleration or velocity was recorded simultaneously at a maximum of two tower platforms due to the limitation of cable length and number of sensors, as mentioned previously; the LDV sensor provided single-point measurements. Hence, only mode shapes measured by the IR sensor were calculated. In these figures, the stability lines of the first mode are clearer than those corresponding to the

second mode. The reason is that the amplitude of vibration corresponding to the second and higher modes of the wind turbine tower was significantly small compared to that of the first mode. In the case of the IR measurement, only the first mode could be identified because of the low precision of the IR sensor in the high-frequency range. The identified frequencies and damping ratios of the wind turbine towers are gathered in Fig. 24.

The mode shapes identified with IR measurements are shown in Figs. 22 and 23. The IR measurements were suitable to extract mode shapes because simultaneous vibration measurements at multiple points at different heights were allowed and spatially dense mode shape measurements were provided. However, IR measurements were only accurate for the first mode here due to the small amplitude of vibration associated with second and higher modes, as discussed previously. In addition, the IR sensor could not be used to obtain the mode shape at the top of the towers because of the interference of the turbine blades. As a result, the mode shapes experimentally extracted only reached the first 40 m of the towers in this work.

Field test results were also compared with FE analysis results. FE models of the two towers were built with beam elements by

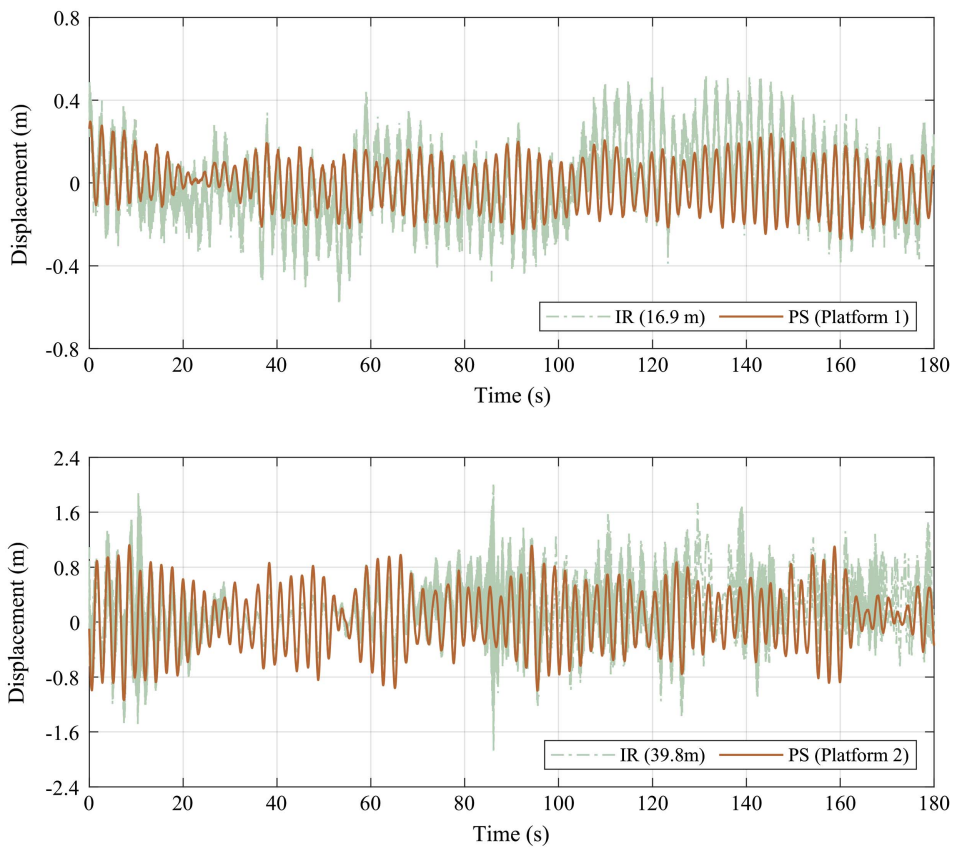


Fig. 17. Synchronized IR measurements and PS measurements in Tower B.

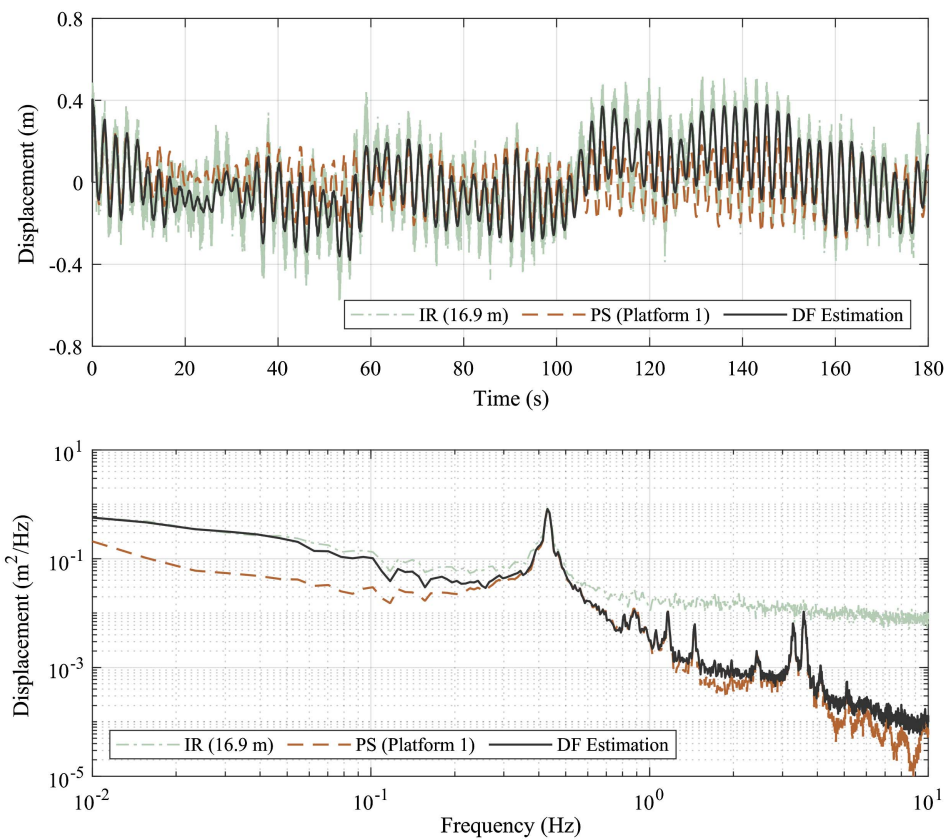


Fig. 18. Time and frequency domain comparison of measurements obtained from IR sensor, PS velocimeters, and data fusion (Platform 1 of Tower B).

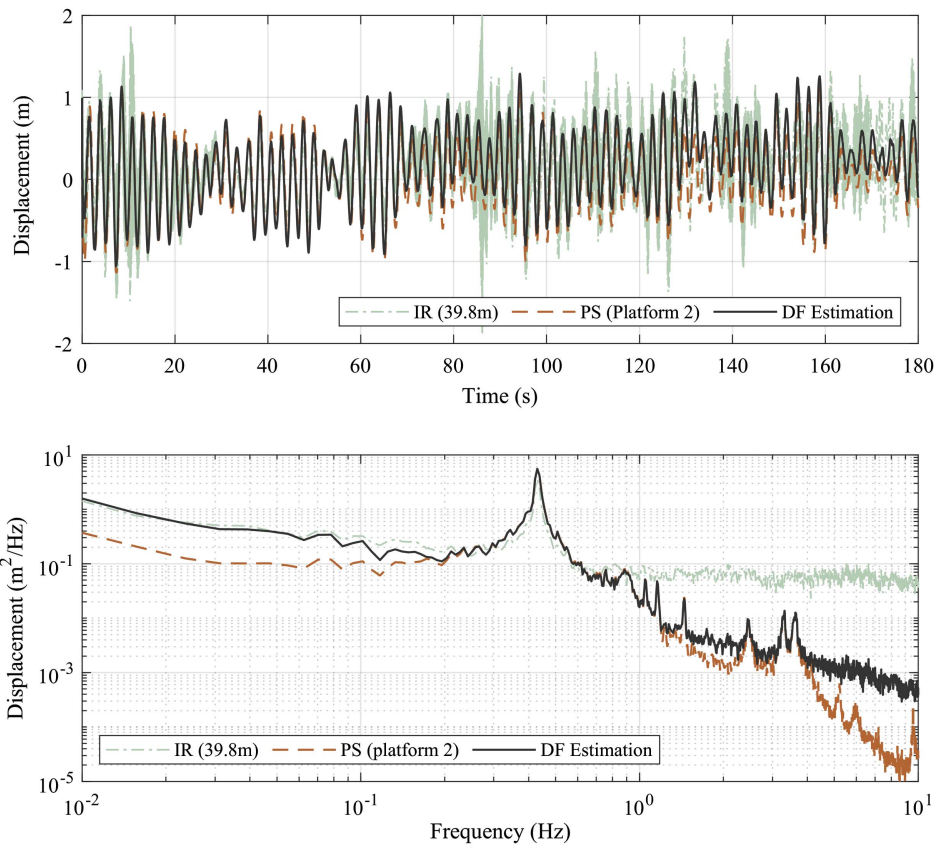


Fig. 19. Time and frequency domain comparison of measurements obtained from IR sensor, PS velocimeters, and data fusion (Platform 2 of Tower B).

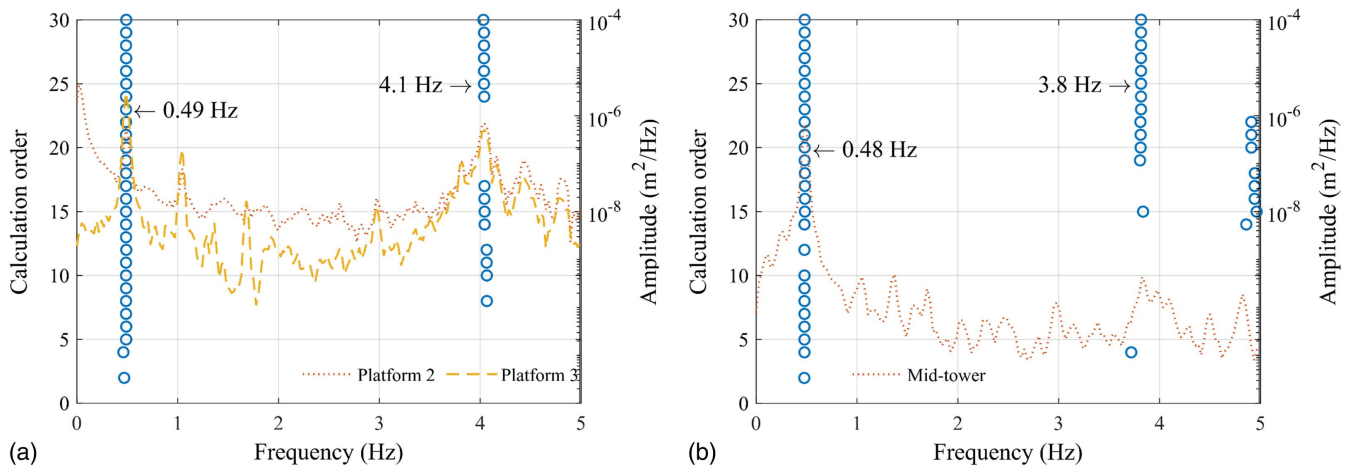


Fig. 20. Stability diagrams obtained from vibration measurements recorded experimentally in Tower A with: (a) IEPE accelerometers; and (b) LDV sensor.

using BEAM188 to represent the tower wall and lumped mass elements by using MASS21 to represent the mass of both the generator and the blades. The foundation was simulated with fixed boundary conditions at the tower bottom. The first two vibration mode FE analysis results for both towers are shown in Fig. 24 for comparison. The results showed that the first-mode frequencies identified experimentally and with FE analysis were very close to one another in both towers. The second-mode frequencies obtained with FE models were marginally higher than those

extracted from experimental vibration measurements. The first mode shapes obtained from FE analysis are also compared to those extracted experimentally with IR measurements for each tower in Figs. 22 and 23. The results showed a good agreement between the first mode shape obtained from the experiments and FE model.

The similarity between the calculated FE mode shapes and the mode shapes identified experimentally is quantified by the modal assurance criterion (MAC)

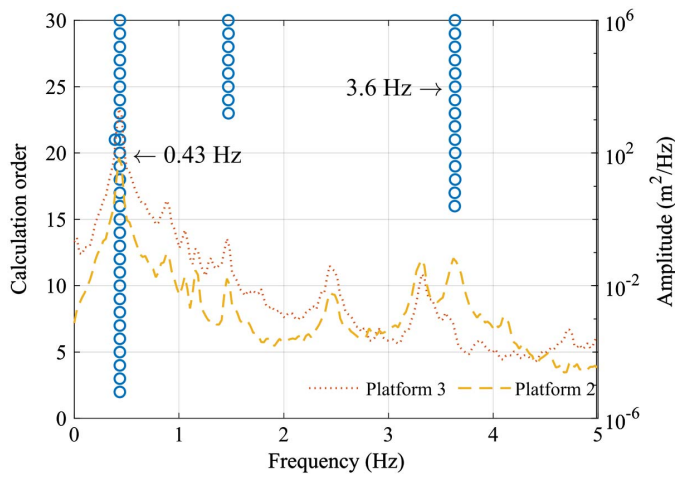


Fig. 21. Stability diagram obtained from vibration measurements recorded experimentally with PS velocimeters in Tower B.

$$MAC = \frac{|\boldsymbol{\varphi}_I^T \boldsymbol{\varphi}_{FE}|^2}{\boldsymbol{\varphi}_I^T \boldsymbol{\varphi}_I \boldsymbol{\varphi}_{FE}^T \boldsymbol{\varphi}_{FE}} \quad (4)$$

where $\boldsymbol{\varphi}_I$ = mode shape identified from experimental results; and $\boldsymbol{\varphi}_{FE}$ = mode shape obtained in FE analysis. The similarity between $\boldsymbol{\varphi}_I$ and $\boldsymbol{\varphi}_{FE}$ increases with the MAC, and it takes the value of 1.0 if the mode shapes obtained experimentally and numerically are identical. In this work, the values of the MAC obtained for tower heights below 40 m were 0.972 and 0.967 in Towers A and B, respectively, which indicates that the comparison of the first modes of the two towers compare well with those from FE models.

The damping ratios can only be obtained by field tests. Although the damping ratios identified with different measurements were not identical, they were all relatively low (those corresponding to the first modes were no more than 2%, and those to the second modes were no more than 3%), which agreed with former experiences (Hu et al. 2015a, b).

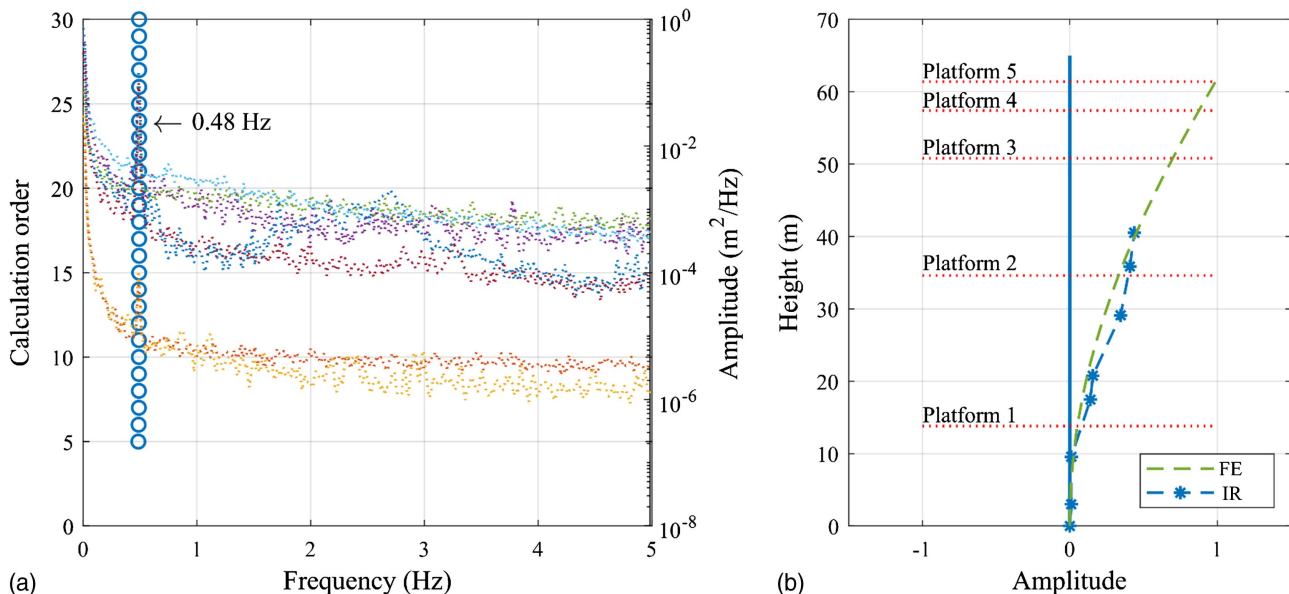


Fig. 22. (a) Stability diagram; and (b) first mode shape in Tower A obtained with IR sensor and FE analysis.

Conclusions and Discussions

This research for this paper studied vibration measurements of two wind turbine towers by using contact and noncontact sensors. The contact sensors included IEPE accelerometers and PS velocimeters; the noncontact sensors included an LDV sensor and an IR sensor. Suitability of these sensors for vibration measurements of the wind turbine towers were compared.

Modal parameters, including frequencies and damping ratios of wind turbine towers, were obtained by using recorded measurements. The results showed that the different types of sensors were able to capture accurately the first frequencies of the wind turbine towers. The first two vibration frequencies of both towers obtained with field measurements, particularly the first ones, were close to those obtained numerically through FE models built from engineering drawings.

Although contact sensors generally failed to record low-frequency vibrations, they gave the most precise vibration measurements for the wind turbine towers, and they are particularly recommended for long-term monitoring in which an installation is permanent. As they are installed in towers for most cases, contact sensors are suitable for wind turbine tower measurements in both working and nonworking conditions. Leaving aside the cost, non-contact sensors, i.e., LDV and IR sensors, significantly simplify testing onsite, because they can be set up at a distance from a tower. In addition, they capture the low-frequency vibration of towers more accurately than contact sensors. However, the quality of the signal recorded by noncontact sensors may be compromised by environmental conditions. The LDV sensor is suitable for one-off monitoring of several towers of wind farms in operation without accessing the towers. It can capture high-order vibration frequencies, well above the first one, with precision comparable to contact sensors. LDV sensors can be used in working conditions by selecting measurement points that are not blocked by obstacles. On the other hand, the use of an IR sensor is recommended to extract mode shapes, because it allows one to obtain a dense array of multipoint measurements from the lower portion of a tower, but not from its top portion due to interference introduced by the blades, and that effect can be stronger in working conditions. Measurements by an IR sensor can only be used to identify first vibration modes,

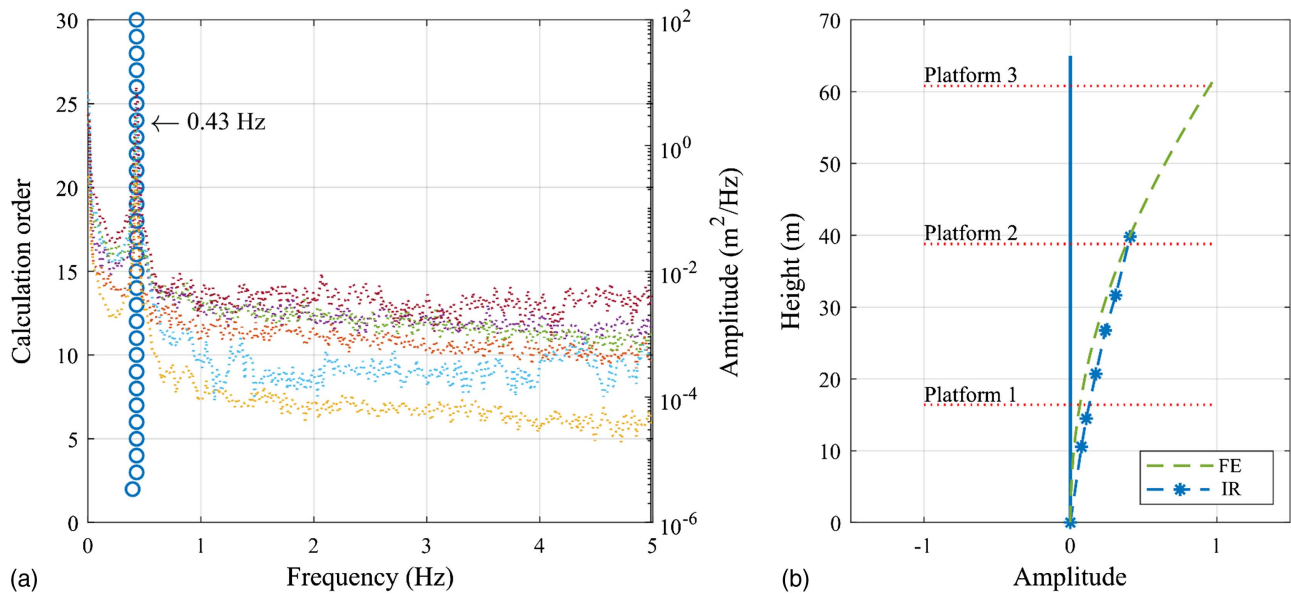


Fig. 23. (a) Stability diagram; and (b) first mode shape in Tower B obtained with IR sensor and FE analysis.




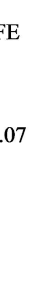
Tower	A								
Mode order	1 st			2 nd					
Sensor		IEPE	LDV	IR	FE		IEPE	LDV	FE
Frequency (Hz)		0.49	0.48	0.49	0.48		4.1	3.8	5.07
Damping ratio		2%	2%	1%			3%	3%	
Tower	B								
Mode order	1 st			2 nd					
Sensor		PS		IR	FE		PS	FE	
Frequency (Hz)		0.43		0.43	0.44		3.6	4.17	
Damping ratio		1%		2%			1%		

Fig. 24. Identified modal parameters in Towers A and B.

because its output is in the form of displacement that has small amplitudes at high-order modes; the quality of the IR sensor output is poor in the high-frequency range. A DF method can be used to get a wide frequency range displacement by combining the superior frequency ranges from different types of sensors. This assertion extends the applicability of an IR sensor, which could be used in the structural health monitoring of wind turbine towers that have permanent contact-sensors installed, particularly if they have tall

towers for which the low dominant vibration frequencies could not be accurately identified if only contact sensors are used.

For long-time vibration monitoring of engineering structures, such as operating wind turbine towers, the use of contact sensors should be considered as the first choice due to their high precision and low cost. For short-term vibration tests, the use of noncontact sensors are preferable if they are available, because they can be easily set up and collect relatively precise vibration measurements.

In addition, most noncontact sensors are capable of measuring vibrations at frequencies lower than 0.25 Hz, which cannot be well handled by most contact sensors. Comparing the two types of noncontact sensors discussed in this paper, i.e., LDV and IR sensors, one can conclude that measurements by an LDV sensor have higher precision and wider frequency range, whereas an IR sensor is capable of simultaneous, multi-point measurements. Note that measurements by the LDV and IR sensors can be interrupted by obstacles between a structure and the sensors, such as the rotating blades of a wind turbine. The findings reported herein are based on the sensor models of IEPE accelerometers, PS velocimeters, LDV sensor, and IR sensor adopted for this study.

Acknowledgments

The authors would like to acknowledge the support from International Collaboration Program of Science and Technology Commission of Ministry of Science and Technology, China (2016YFE0105600); International Collaboration Program of Science and Technology Commission of Shanghai Municipality and Sichuan Province (16510711300 and 18GJHZ0111); 111 Project (B18062); National Natural Science Foundation of China (U1710111 and 51878426); Fundamental Research Funds for Central Universities of China; National Science Foundation (CMMI-1763024 and CMMI-1762917); and China Scholarship Council.

References

Brownjohn, J. M. W., Y. Xu, and D. Hester. 2017. "Vision-based bridge deformation monitoring." *Front. Built Environ.* 3: 23. <https://doi.org/10.3389/fbuil.2017.00023>.

Chou, J.-S., and W.-T. Tu. 2011. "Failure analysis and risk management of a collapsed large wind turbine tower." *Eng. Fail. Anal.* 18 (1): 295–313. <https://doi.org/10.1016/j.engfailanal.2010.09.008>.

Dai, K., Y. Huang, C. Gong, Z. Huang, and X. Ren. 2015. "Rapid seismic analysis methodology for in-service wind turbine towers." *Earthquake Eng. Eng. Vib.* 14 (3): 539–548. <https://doi.org/10.1007/s11803-015-0043-0>.

Dai, K., C. Sheng, Z. Zhao, Z. Yi, A. Camara, and G. Bitsuamlak. 2017a. "Nonlinear response history analysis and collapse mode study of a wind turbine tower subjected to tropical cyclonic winds." *Wind Struct.* 25 (1): 79–100. <https://doi.org/10.12989/was.2017.25.1.079>.

Dai, K., Y. Wang, Y. Huang, W. Weidong Zhu, and Y. Xu. 2017b. "Development of a modified stochastic subspace identification method for rapid structural assessment of in-service utility-scale wind turbine towers." *Wind Energy* 20 (10): 1687–1710. <https://doi.org/10.1002/we.2117>.

Gentile, C., and A. Cabboi. 2015. "Vibration-based structural health monitoring of stay cables by microwave remote sensing." *Smart Struct. Syst.* 16 (2): 263–280. <https://doi.org/10.12989/sss.2015.16.2.263>.

Golub, G. H., and C. F. Van Loan. 1996. *Matrix computations*. 3rd ed. Baltimore: John Hopkins University Press.

Hu, W.-H., S. Thöns, R. G. Rohrmann, S. Said, and W. Rücker. 2015a. "Vibration-based structural health monitoring of a wind turbine system. Part I: Resonance phenomenon." *Eng. Struct.* 89 (Apr): 260–272. <https://doi.org/10.1016/j.engstruct.2014.12.034>.

Hu, W.-H., S. Thöns, R. G. Rohrmann, S. Said, and W. Rücker. 2015b. "Vibration-based structural health monitoring of a wind turbine system. Part II: Environmental/operational effects on dynamic properties." *Eng. Struct.* 89 (Apr): 273–290. <https://doi.org/10.1016/j.engstruct.2014.12.035>.

IDS GeoRadar Inc. 2016. *IBIS-FS & IBIS-FS plus user manual*. Ospedaletto, Italy: IDS GeoRadar.

Kim, K., and H. Sohn. 2017. "Dynamic displacement estimation by fusing LDV and LiDAR measurements via smoothing based Kalman filtering." *Mech. Syst. Sig. Process.* 82 (Jan): 339–355. <https://doi.org/10.1016/j.ymsp.2016.05.027>.

Li, J., Z. Zhang, and J. Chen. 2012. "Experimental study on vibration control of offshore wind turbines using a ball vibration absorber." *Energy Power Eng.* 4 (3): 153–157. <https://doi.org/10.4236/epe.2012.43021>.

Luzi, G., M. Crosetto, and O. Monserrat. 2014. "Monitoring a tall tower through radar interferometry: The case of the Collserola tower in Barcelona." In Vol. 1600 of *Proc., AIP Conf.*, 171–179. <https://doi.org/10.1063/1.4879579>.

Ozbek, M., and D. J. Rixen. 2013. "Operational modal analysis of a 2.5 MW wind turbine using optical measurement techniques and strain gauges." *Wind Energy* 16 (3): 367–381. <https://doi.org/10.1002/we.1493>.

Peeters, B., and G. De Roeck. 1999. "Reference-based stochastic subspace identification for output-only modal analysis." *Mech. Syst. Sig. Process.* 13 (6): 855–878. <https://doi.org/10.1006/mssp.1999.1249>.

Pieraccini, M. 2013. "Monitoring of civil infrastructures by interferometric radar: A review." *Sci. World J.* 2013: 786961. <https://doi.org/10.1155/2013/786961>.

Pieraccini, M., F. Parrini, M. Fratini, C. Atzeni, and P. Spinelli. 2008. "In-service testing of wind turbine towers using a microwave sensor." *Renewable Energy* 33 (1): 13–21. <https://doi.org/10.1016/j.renene.2007.02.001>.

Polytec Inc. 2017. "Datasheet of Polytec RSV-150." Accessed January 12, 2017. <https://www.polytec.com/eu/>.

Swartz, R., J. Lynch, S. Zerbst, B. Sweetman, and R. Rolfes. 2010. "Structural monitoring of wind turbines using wireless sensor networks." *Smart Struct. Syst.* 6 (3): 183–196. <https://doi.org/10.12989/sss.2010.6.3.183>.

Van Overschee, P., and B. De Moor. 1993. "Subspace algorithms for the stochastic identification problem." *Automatica*. 29 (3): 649–660. [https://doi.org/10.1016/0005-1098\(93\)90061-W](https://doi.org/10.1016/0005-1098(93)90061-W).

Yang, Q., L. Lou, and L. Yang. 2005. "Model 941B ultra-low frequency vibration gauge." [In Chinese.] *Earthquake Eng. Eng. Vib.* 25 (04): 174–179.

Zhang, R., Z. Zhao, and K. Dai. 2019. "Seismic response mitigation of a wind turbine tower using a tuned parallel inerter mass system." *Eng. Struct.* 180 (Feb): 29–39. <https://doi.org/10.1016/j.engstruct.2018.11.020>.

Zhao, Z., K. Dai, A. Camara, G. Bitsuamlak, and C. Sheng. 2019. "Wind turbine tower failure modes under seismic and wind loads." *J. Perform. Constr. Facil.* 33 (2): 04019015. [https://doi.org/10.1061/\(ASCE\)CF.1943-5509.0001279](https://doi.org/10.1061/(ASCE)CF.1943-5509.0001279).